




Bound-state stability of Coulomb three-body systems using numerical tensor methodsKammegne Tcheugam Brice ^{1,2}, Michael Melgaard ^{1,*} and Hazel Cox ^{2,†}¹*Department of Mathematics, University of Sussex, Brighton BN1 9QJ, United Kingdom*²*Department of Chemistry, University of Sussex, Falmer, Brighton BN1 9QJ, United Kingdom*

(Received 28 January 2024; revised 26 April 2024; accepted 20 May 2024; published 24 June 2024)

In this paper we present a unified treatment of three-body atoms and molecules using numerical tensor methods. The Schrödinger equation in perimetric coordinates is recast in a canonical tensor format. It is shown that the Schrödinger equation can be solved in this full-tensor format but that by using a low-rank tensor decomposition, in particular the tensor-train and quantized-tensor-train formats, energies accurate to at least the nanohartree can be obtained for the He atom (in which the mass of the uniquely charged particle is much greater than the other two particles), the positronium negative ion (Ps^- , in which all the masses are equal), and the non-Born-Oppenheimer H_2^+ molecule (in which the mass of the uniquely charged particle is much smaller than the other two particles).

DOI: [10.1103/PhysRevA.109.062812](https://doi.org/10.1103/PhysRevA.109.062812)**I. INTRODUCTION**

Computational quantum chemistry (QC) has developed into an indispensable and versatile tool, providing quantitative data and new understanding of chemical systems and processes in chemistry and large parts of physics. However, as the many-particle Schrödinger equation (SE) cannot be solved exactly, approximations are necessary. The standard QC approach is to apply the Born-Oppenheimer (BO) approximation and solve the electronic Schrödinger equation in the field of the nuclei. Conventional QC methods build on the Hartree-Fock (HF) description, which is then refined by introducing electronic excitations into a set of virtual (unoccupied) molecular orbitals culminating in full-configuration interaction (FCI). In the limit of a complete basis set and excitations of all the electrons into all the virtual orbitals, the exact numerical solution of the nonrelativistic time-independent SE is obtained. However, FCI scales exponentially in floating-point operations and memory with the size of the system.

An extremely powerful method that has emerged that tackles the exponentially greater cost in both computation and memory with increasing excitations in coupled-cluster or CI theory is the density-matrix renormalization-group (DMRG) method which exploits the full power of tensors. It arose in the physics community but has been successfully applied to the field of QC. QC-DMRG allows the FCI wave function to be approximated to a desired accuracy with a reasonable cost by defining a matrix product state (MPS) as a low-rank decomposition of the FCI tensor using a suitable finite single-particle basis. Implementations of QC-DMRG build on the

underlying tensor structure, in which both the MPS [known as a tensor train (TT) in mathematics] representing the variational state, as well as the Hamiltonian operator converted to a matrix product operator (MPO), are represented as tensor networks. The accuracy of the DMRG method essentially depends on the bond dimension (TT rank), which corresponds to the number of renormalized states [1]. Without reduction of the rank, DMRG scales exponentially, but with the choice of a suitable bond dimension the computational complexity is reduced to polynomial scaling. There are many excellent reviews on DMRG (see, for example, [2–5] and references therein).

An alternative approach to globally defined trial wave functions is to solve the system using numerical methods on a mesh. For example, in the finite-element method (FEM) the wave function is approximated using piecewise, locally defined interpolation functions. The domain is segmented into the chosen elements (e.g., tetrahedra, cubes, etc.), and a basis of local functions, continuous over the whole domain, is defined in each element. The quality of finite-element approximations depends on the form and the density of the mesh involved. In a series of papers, Levin, Ford, Shertzer, and Ackermann [6–10] demonstrated that FEM can be used to calculate accurate ground-state energies for three-body Coulomb systems. Although the resulting matrices are sparse, the high matrix dimensions needed for high accuracy presented a bottleneck. However, over the past few decades, there has been growth in electronic structure codes using real-space numerical methods on an adaptive mesh (see, for example, [11]). This has facilitated massively parallel real-space code for large-scale density-functional-theory calculations based on adaptive finite-element discretization [12].

The motivation for and emphasis on the development of numerical tensor methods (NTMs) within the mathematics and scientific computing community result from the desire to overcome the exponential growth in complexity with the number of degrees of freedom, known as the “curse of dimensionality,” that plagues the computation of eigenvalues in higher dimensions. Such high-dimensional problems arise

*Contact author: m.melgaard@sussex.ac.uk†Contact author: h.cox@sussex.ac.uk

in various applications in physics, chemistry, biology, and engineering. Of note for the present work are the developments by Khoromskaia and Khoromskij which culminated in their book *Tensor Numerical Methods in Quantum Chemistry* [13], in which they developed a NTM to solve the HF equations using Gaussian-type basis functions discretized on three-dimensional Cartesian grids and a Tucker tensor decomposition. Later, this grid representation of the basis functions was generalized to any well-separable function defined on a grid. They were able to show that their NTMs, based on efficient rank-structured tensor representations of the multivariate functions and operators on a Cartesian grid, break the curse of dimensionality. An alternative formulation was used by Veit and Scott [14]. They used a finite-element approach in combination with a low-rank TT approach when considering the SE for two hydrogen atoms with a large separation within the BO approximation.

The purpose of this paper is to solve the all-particle time-independent Schrödinger equation for any three-body Coulomb system using numerical tensor methods. Although the cornerstone of QC and molecular physics is the BO approximation, for few-particle systems it is possible to formulate methods which treat the electrons and nuclei on equal footing, and thus, the BO approximation is not invoked (see, for example, [15–18]). These fully correlated all-particle methods, referred to as non-BO or pre-BO, can provide high-accuracy energies and wave functions. In general, in such non-BO calculations, the Hamiltonian matrix must take all particles into account, which leads to an exponential growth of its dimension with the number of degrees of freedom and hence is limited to few-particle systems. Here we show that for three-body systems, by using perimetric coordinates which are linear combinations of the interparticle coordinates, we can write the wave function in terms of separable functions, allowing us to recast the SE in canonical tensor format. Rather than discretizing a globally analytical wave function or using globally defined functions, we start instead by using a finite-element approach. We choose our shape or basis functions to be Lagrange interpolation functions, select nodes on a grid in the three-dimensional space spanned by the perimetric coordinates, and hence express the operators in the SE in canonical tensor format. To reduce the computational complexity we convert the SE to TT format and, subsequently, a quantized-tensor-train (QTT) format and optimize a low-rank representation using a DMRG-type algorithm known as the alternating linear scheme (ALS) [19], which is implemented within the TT toolbox written by Gelß *et al.* [20,21]. It is shown that energies of at least nanohartree accuracy can be obtained for an all-particle treatment of an atomic system (where the mass of the uniquely charged particle m_3 is much greater than those of the other two particles, m_1 and m_2 , i.e., $m_3 \gg m_1, m_2$), an exotic system (Ps^- , where $m_1 = m_2 = m_3$), and a molecular system (where $m_1, m_2 \gg m_3$).

II. TENSORS

In this paper, tensors are simply multidimensional generalizations of matrices, represented by arrays with d indices,

corresponding to an element of a tensor product of d vector spaces. First-order tensors (that is, vectors) are usually denoted by lowercase boldface letters ($\mathbf{a}, \mathbf{b}, \mathbf{c}, \dots$), second-order tensors (matrices) are denoted by capital letters ($\mathbf{A}, \mathbf{B}, \mathbf{C}, \dots$), and higher-order tensors are denoted by calligraphic letters ($\mathcal{S}, \mathcal{T}, \mathcal{U}, \dots$). The *order* of a tensor is the number of dimensions, also known as *ways* or *modes*. A d th-order tensor $\mathcal{T} \in \mathbb{R}^N = \mathbb{R}^{n_1 \times n_2 \times \dots \times n_d}$, where $n_i \in \mathbb{N}$ for $i = 1, 2, \dots, d$, $d \in \mathbb{N}$, can be represented in its full format in terms of its entries t_{x_1, \dots, x_d} by

$$\mathcal{T} = [\mathcal{T}(x_1, \dots, x_d)] = [t_{x_1, \dots, x_d}], \quad x_i \in \{1, 2, \dots, n_i\}, \\ i = 1, 2, \dots, d. \quad (1)$$

We call $N = (n_1, \dots, n_d)^T \in \mathbb{R}^d$ the mode set or index set.

Definition 1 [21]. A tensor $\mathcal{T} \in \mathbb{R}^N$, $\mathbb{R}^N = \mathbb{R}^{n_1 \times \dots \times n_d}$, of order d is called a rank-1 tensor if it can be written as the tensor product of d vectors, i.e.,

$$\mathcal{T} = \bigotimes_{i=1}^d \mathbf{T}^{(i)} = \mathbf{T}^{(1)} \otimes \dots \otimes \mathbf{T}^{(d)}, \quad (2)$$

where $\mathbf{T}^{(i)} \in \mathbb{R}^{n_i}$ for $i = 1, \dots, d$.

If we consider linear operators $\mathcal{G} \in \mathbb{R}^{M \times N}$, with $\mathbb{R}^{M \times N} = \mathbb{R}^{(m_1 \times n_1) \times \dots \times (m_d \times n_d)}$, that can be expressed as rank-1 tensors, the components $\mathcal{G}^{(i)}$ are matrices, i.e.,

$$\mathcal{G} = \bigotimes_{i=1}^d \mathcal{G}^{(i)} = \mathcal{G}^{(1)} \otimes \dots \otimes \mathcal{G}^{(d)}, \quad (3)$$

with $\mathcal{G}^{(i)} \in \mathbb{R}^{m_i \times n_i}$ for $i = 1, \dots, d$.

A. Canonical polyadic decomposition

The idea of the canonical (polyadic) format is to express a tensor as the sum of a finite number of rank-1 tensors (see, e.g., [22,23]). We give the definition for tensor operators (see, e.g., Kolda and Bader [22] and Hackbusch [23]), and we use the notation from Gelß [21]. When we fix certain indices, colons are used to indicate the free modes (compare with MATLAB [24] colon notation).

Definition 2. A tensor operator $\mathcal{G} \in \mathbb{R}^{M \times N}$, with $\mathbb{R}^{M \times N} = \mathbb{R}^{(m_1 \times n_1) \times \dots \times (m_d \times n_d)}$, is said to be in the canonical format if

$$\mathcal{G} = \sum_{k=1}^r \bigotimes_{i=1}^d \mathcal{G}_{k, :, :}^{(i)} = \sum_{k=1}^r \mathcal{G}_{k, :, :}^{(1)} \otimes \dots \otimes \mathcal{G}_{k, :, :}^{(d)}, \quad (4)$$

with cores $\mathcal{G}^{(i)} \in \mathbb{R}^{r \times m_i \times n_i}$ and $\mathcal{G}_{k, :, :}^{(i)} \in \mathbb{R}^{m_i \times n_i}$ for all $k \in \{1, \dots, r\}$ and $i \in \{1, \dots, d\}$, where r is called the canonical rank of the decomposition.

The canonical decomposition is the simplest and most natural extension of the idea of the singular-value matrix decomposition, and any tensor can be represented by a linear combination of elementary tensors as in (2). However, the number r of required rank-1 tensors play an important role, and moreover, the set of canonical tensors with bounded rank do not form a manifold, and as a consequence, optimization problems can be ill posed [25]. Due to such drawbacks many attempts have been made to find more stable, if perhaps more complex, decompositions. Decompositions that require $O(d)$ values to exactly recreate a d th-order

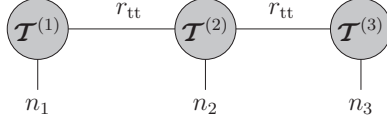


FIG. 1. Tensor-train representation for $\mathcal{T} \in \mathbb{R}^N$, with TT ranks $r_1 = r_2 = r_{tt}$.

tensor are clearly desirable. One such decomposition is the TT decomposition or, more commonly, TT format. The TT format is similar to the singular-value decomposition in that it uses products of matrices to approximate the full tensor.

B. Tensor-train decomposition

A tensor in the TT format can be written as a matrix product (compare with MPSs [26,27]). The mathematics was formally developed by Hackbusch and Kühn [28] and Oseledets and Tyrtyshnikov [29] in 2009 as a useful tool for numerical computations due to its stability from an algorithmic point of view and reasonable computational cost; we refer to Oseledets [30] and Hackbusch [23], adopting again the notation in the work of Gelß [21].

Definition 3. Given a tensor $\mathcal{T} \in \mathbb{R}^N = \mathbb{R}^{n_1 \times \dots \times n_d}$, the TT format for \mathcal{T} has d third-order core (or factor) tensors $\mathcal{T}^{(k)} \in \mathbb{R}^{r_{k-1} \times n_k \times r_k}$, where $(r_1, \dots, r_{d-1}) \in \mathbb{N}^{d-1}$ and $r_0 = r_d = 1$, such that

$$\begin{aligned} \mathcal{T} &= \sum_{k=0}^{r_0} \dots \sum_{k_d=1}^{r_d} \bigotimes_{k_i=1, \dots, k_i} \mathcal{T}_{k_i-1, \dots, k_i}^{(i)} \\ &= \sum_{k=0}^{r_0} \dots \sum_{k_d=1}^{r_d} \mathcal{T}_{k_0, \dots, k_1}^{(1)} \otimes \dots \otimes \mathcal{T}_{k_{d-1}, \dots, k_d}^{(d)}, \end{aligned} \quad (5)$$

where the numbers r_k are called TT ranks. Likewise, a tensor operator $\mathcal{G} \in \mathbb{R}^{M \times N}$, with $\mathbb{R}^{M \times N} = \mathbb{R}^{(m_1 \times n_1) \times \dots \times (m_d \times n_d)}$, is said to be in the TT format if

$$\begin{aligned} \mathcal{G} &= \sum_{k=0}^{R_0} \dots \sum_{k_d=1}^{R_d} \bigotimes_{i=1}^d \mathcal{G}_{k_i-1, \dots, k_i}^{(i)} \\ &= \sum_{k=0}^{R_0} \dots \sum_{k_d=1}^{R_d} \mathcal{G}_{k_0, \dots, k_1}^{(1)} \otimes \dots \otimes \mathcal{G}_{k_{d-1}, \dots, k_d}^{(d)}, \end{aligned} \quad (6)$$

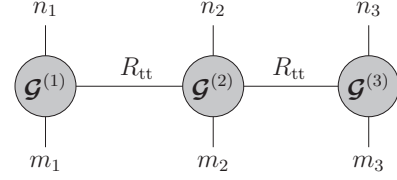


FIG. 2. Tensor-train operator representation for $\mathcal{G} \in \mathbb{R}^{M \times N}$, with TT ranks $R_1 = R_2 = R_{tt}$.

with TT cores $\mathcal{G}^{(i)} \in \mathbb{R}^{R_{i-1} \times m_i \times n_i \times R_i}$ for $i = 1, \dots, d$ and $R_0 = R_d = 1$; the numbers R_i are called the TT ranks of the operator cores.

Figure 1 shows the graphical representation of a tensor train associated with a third-order tensor $\mathcal{T} \in \mathbb{R}^N$ with TT ranks $r_1 = r_2 = r_{tt}$, and the diagram in Fig. 2 illustrates a tensor-train operator associated with a third-order tensor operator $\mathcal{G} \in \mathbb{R}^{M \times N}$ with TT ranks $R_1 = R_2 = R_{tt}$.

Throughout our calculations, the number of nodes n (for each mode) proves to be a limiting factor within the full-tensor format since each operator has elements of $\mathbb{R}^{n^3 \times n^3}$. To ensure high accuracy, it is essential to have a sufficient number of nodes. This is where the application of the TT format becomes highly beneficial, as it dramatically reduces computational complexity (storage, CPU time, memory, and processing).

C. Quantized tensor train

We can also quantize the TT format if the mode lengths n_i can be written as a product of many integers (prime integers, for example). This quantization procedure is called a QTT [31], and it proves to be advantageous, particularly in the context of the ALS algorithm [19]. During each iteration of ALS, the algorithm tackles microeigenvalue problems using reduced matrix dimensions; as a result, computations become faster even if they require higher ranks for the initial guess.

We briefly explain this concept for third-order tensors. Let us assume

$$n_i = \prod_{j=1}^{q_i} n_{i,j},$$

where q_i is the number of integers (different from 1) appearing in the decomposition of n_i . So if

$$N = M = \left[\prod_{j=1}^{q_1} n_{1,j}, \prod_{j=1}^{q_2} n_{2,j}, \prod_{j=1}^{q_3} n_{3,j} \right],$$

then we can define the corresponding quantization

$$\mathbf{G}' \in \mathbb{R}^{(n_{1,1} \times n_{1,1}) \times \dots \times (n_{1,q_1} \times n_{1,q_1}) \times (n_{2,1} \times n_{2,1}) \times \dots \times (n_{2,q_2} \times n_{2,q_2}) \times (n_{3,1} \times n_{3,1}) \times \dots \times (n_{3,q_3} \times n_{3,q_3})}$$

by

$$\mathbf{G}'_{x_{1,1}, y_{1,1}, \dots, x_{1,q_1}, y_{1,q_1}, x_{2,1}, y_{2,1}, \dots, x_{2,q_2}, y_{2,q_2}, x_{3,1}, y_{3,1}, \dots, x_{3,q_3}, y_{3,q_3}} = \mathbf{G}_{x_1, y_1, \dots, x_d, y_d},$$

where, using the little-endian convention [21], $x_i = \overline{x_{i,1} \dots x_{i,q_i}}$ and $y_i = \overline{y_{i,1} \dots y_{i,q_i}}$ for $i = 1, 2, 3$. See Fig. 3,

where we illustrate the concept adapted to our particular case (note that, in Fig. 3, $p_j := n_{1,j} = n_{2,j} = n_{3,j}$). The TT

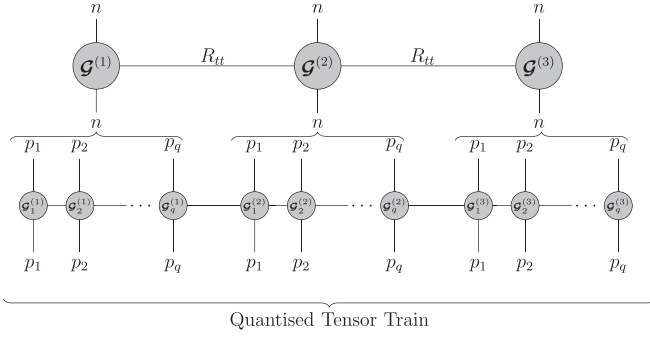


FIG. 3. Conversion from TT to QTT format of an operator: Each core is divided into several cores with smaller mode sizes.

rank of the wave function is not affected by the quantization procedure of the operators, and thus, the QTT rank is that defined by the TT rank of the wave function (see Sec. II B).

III. THREE-BODY SCHRÖDINGER EIGENVALUE PROBLEM

We consider the motion of three charged point particles with masses m_i and charges Z_i , $i = 1, 2, 3$. After separating the center-of-mass motion and taking the origin to be the location of particle 3, the time-independent Schrödinger equation for the system is given by

$$H\psi = E\psi, \quad \psi \neq 0, \quad (7)$$

where the Hamiltonian (Schrödinger) operator takes the form (see, e.g., [32,33])

$$H = -\frac{1}{2\mu_1}\nabla_1^2 - \frac{1}{2\mu_2}\nabla_2^2 - \frac{1}{m_3}\nabla_1 \cdot \nabla_2 + \frac{Z_1Z_3}{r_1} + \frac{Z_2Z_3}{r_2} + \frac{Z_1Z_2}{r_{12}}, \quad (8)$$

with r_1 and r_2 being the interparticle distances with respect to the third particle, r_{12} being the distance between particles 1 and 2, and $\mu_i^{-1} = m_i^{-1} + m_3^{-1}$, $i = 1, 2$. Despite their geometrical significance, being the sides of a triangle, the domains of the variables are not independent due to the triangular condition, which creates difficulties in the calculation of the Hamiltonian matrix elements. For this reason, Coolidge and James [34] introduced the perimetric coordinates z_i , $i = 1, 2, 3$, which are linear combinations of the interparticle coordinates:

$$z_1 = r_2 + r_{12} - r_1, \quad (9a)$$

$$z_2 = r_{12} + r_1 - r_2, \quad (9b)$$

$$z_3 = r_1 + r_2 - r_{12}. \quad (9c)$$

The linear transformations in (9) facilitate our calculations since each variable ranges from 0 to ∞ . In the new coordinate system, straightforward use of the chain rule of differentiation yields the following form of the SE (7) in atomic units (see

[35,36]):

$$-\frac{1}{2}\left(v_{11}\frac{\partial^2\psi}{\partial z_1^2} + v_{22}\frac{\partial^2\psi}{\partial z_2^2} + v_{33}\frac{\partial^2\psi}{\partial z_3^2} + v_1\frac{\partial\psi}{\partial z_1} + v_2\frac{\partial\psi}{\partial z_2} + v_3\frac{\partial\psi}{\partial z_3} + v_{12}\frac{\partial^2\psi}{\partial z_1\partial z_2} + v_{23}\frac{\partial^2\psi}{\partial z_2\partial z_3} + v_{13}\frac{\partial^2\psi}{\partial z_1\partial z_3}\right) + V\psi = E\psi, \quad (10)$$

where

$$V = \frac{2Z_1Z_2}{z_1 + z_2} + \frac{2Z_2Z_3}{z_2 + z_3} + \frac{2Z_3Z_1}{z_3 + z_1} \quad (11)$$

and

$$v_i = 4\left(\frac{-1}{\mu_i(z_j + z_k)} + \frac{1}{\mu_j(z_i + z_k)} + \frac{1}{\mu_k(z_i + z_j)}\right),$$

$$v_{ii} = \frac{1}{\mu_1} + \frac{1}{\mu_2} + \frac{1}{\mu_3} - \frac{b_{ij}}{\mu_{ij}} - \frac{b_{ik}}{\mu_{ik}} + \frac{b_{jk}}{\mu_{jk}},$$

$$v_{ij} = 2\left(-\frac{1}{\mu_i} - \frac{1}{\mu_j} + \frac{1}{\mu_k} + \frac{b_{ij}}{\mu_{ij}}\right),$$

$$b_{ij} = 2\left(\frac{x - 2z_i z_j(z_i + z_j)}{x}\right),$$

$$x = (z_1 + z_2)(z_2 + z_3)(z_3 + z_1). \quad (12)$$

Here x arises from the internal coordinate part of the Jacobian, which is equal to $x/8$ for the transformation to perimetric coordinates.

Definition 4. Strong solution. Let $\Theta = (0, \infty)^3$. An eigenpair $(\psi, E) \in C^2(\Theta) \times \mathbb{R}$ is a strong solution of the Schrödinger eigenvalue problem (7) in perimetric coordinates if (10) holds.

Next, we multiply both sides of Eq. (10) by a smooth, compactly supported (test) function ϕ . Then we integrate over the whole space on both sides, and subsequently, we perform an integration by parts on the left-hand side, multiplying through by the Jacobian, where x is defined in (12). After simplifying the resulting expression, we obtain the weak formulation.

Definition 5. Weak solution. An eigenpair $(\psi, E) \in H_0^1(\Theta) \times \mathbb{R}$ is said to be a weak solution of the Schrödinger eigenvalue problem (10) if

$$\int_0^\infty dz_1 \int_0^\infty dz_2 \int_0^\infty dz_3 \left\{ \frac{1}{2} \left[xv_{11} \frac{\partial\psi}{\partial z_1} \frac{\partial\phi}{\partial z_1} + xv_{22} \frac{\partial\psi}{\partial z_2} \frac{\partial\phi}{\partial z_2} + xv_{33} \frac{\partial\psi}{\partial z_3} \frac{\partial\phi}{\partial z_3} + \frac{xv_{12}}{2} \left(\frac{\partial\psi}{\partial z_2} \frac{\partial\phi}{\partial z_1} + \frac{\partial\psi}{\partial z_1} \frac{\partial\phi}{\partial z_2} \right) + \frac{xv_{23}}{2} \left(\frac{\partial\psi}{\partial z_2} \frac{\partial\phi}{\partial z_3} + \frac{\partial\psi}{\partial z_3} \frac{\partial\phi}{\partial z_2} \right) + \frac{xv_{31}}{2} \left(\frac{\partial\psi}{\partial z_3} \frac{\partial\phi}{\partial z_1} + \frac{\partial\psi}{\partial z_1} \frac{\partial\phi}{\partial z_3} \right) \right] + x(V - E)\psi\phi \right\} = 0 \quad (13)$$

for all test functions $\phi \in H_0^1(\Theta)$, the Sobolev space of order 1. The space arises by taking the completion of $C_0^\infty(\Theta)$ with respect to the $H^1(\Theta)$ norm.

The variational form of the eigenvalue problem (13) is as follows: find an eigenpair $(\psi, E) \in H_0^1(\Theta) \times \mathbb{R}$ such that (13) holds for all $\phi \in H_0^1(\Theta)$.

IV. DISCRETIZATION AND NUMERICAL TENSOR METHOD

We wish to solve the eigenvalue problem (13) using numerical tensor methods, so we need to express the problem in tensor format.

A. Galerkin problem: Choice of grid and basis functions

To derive the eigenvalue problem (13) in tensor format, we use the Galerkin finite-element scheme. For this purpose, we begin by constructing a grid on the truncated domain $\Omega = (0, z_c)^3 \subset \Theta$, where the finite number z_c will be referred to as the cutoff parameter. As the perimetric coordinates are linearly independent, we first define a grid on the interval $(0, z_c) \subset \mathbb{R}$, consisting of the points

$$\zeta_i = ih, \quad h = z_c/(n+1), \quad (14)$$

where $n \in \mathbb{N}$ is the number of nodes in one dimension (i.e., n is the mode length). Associated with this uniform grid is the vector space of piecewise linear polynomials. However, this choice of basis functions leads to poor results. Therefore, Lagrange interpolation functions were chosen. For a given set of uniform points ζ_i in an interval $(0, z_c)$ defined as in (14), at each node we associate a Lagrange polynomial L_i of degree $n-1$ defined by

$$L_i(z) = \prod_{m=1, m \neq i}^n \frac{z - \zeta_m}{\zeta_i - \zeta_m}. \quad (15)$$

For all $1 \leq i \leq n$, we have $L_i \in \mathbb{P}_{n-1}$, the space of polynomials of degree less than or equal to $n-1$, and in order to take into account the Dirichlet conditions at the boundary of $(0, z_c)$, we set

$$V_h := \mathbb{P}_{n-1} \cap H_0^1((0, z_c)),$$

which is a finite-dimensional subspace of $H_0^1(\mathbb{R}_+)$. We then approximate the Sobolev space $H_0^1(\Theta)$ by

$$\mathcal{V}_h := \bigotimes_{k=1}^3 V_h.$$

The accuracy using these basis functions becomes much better than the standard linear hat functions first tried. However, there is a chaotic behavior when $n \geq 12$. This phenomenon is called the ‘‘Runge phenomenon’’ [37], caused by the uniform discretization of $(0, z_c)$. To overcome this problem a nonuniform grid was implemented, in which ζ_i are defined using the Chebyshev node formula [37]

$$\zeta_i = \frac{z_c}{2} + \frac{z_c}{2} \cos \left[\frac{2i-1}{2n} \pi \right], \quad i \in \{1, \dots, n\}. \quad (16)$$

We define the index set $\mathcal{I} := \{1, 2, \dots, n\}^3$ and use bold-face letters for elements in this set, e.g., $\mathcal{I} \ni \mathbf{i} = (i_1, i_2, i_3)$.

Analogous to the one-dimensional case, basis functions for the three-dimensional space \mathcal{V}_h are given by

$$L_i(\mathbf{z}) = \prod_{k=1}^3 L_{i_k}(z_k), \quad (17)$$

where $\mathbf{z} = (z_1, z_2, z_3)$ are the perimetric coordinates in (9). To solve the variational problem (13) numerically, we seek an approximate solution, or ansatz ψ_h , that belongs to the (trial) space \mathcal{V}_h , i.e., an ansatz with the form

$$\psi_h(z_1, z_2, z_3) = \sum_{i \in \mathcal{I}} C_i L_i(\mathbf{z}) = \sum_{i \in \mathcal{I}} C_i L_{i_1}(z_1) L_{i_2}(z_2) L_{i_3}(z_3), \quad (18)$$

where the coefficients C_i are to be determined. To determine the coefficients C_i of the trial function, we impose a finite-dimensional version for the variational problem (13). We demand that (13) holds for ψ_h chosen as in (18) and for all $\phi \in \mathcal{V}_h$. The resulting equations are the Galerkin equations. Since \mathcal{V}_h is finite dimensional, it suffices to impose (13) for ϕ ranging over the elements of a basis for \mathcal{V}_h . Therefore, the Galerkin equations reduce to (a linear system of) the form

$$\mathcal{H}\mathcal{C} = E\mathcal{S}\mathcal{C}, \quad (19)$$

where

$$\mathcal{H} = \langle HL_i, L_k \rangle, \quad \mathcal{S} = \langle L_i, L_k \rangle, \quad \forall \mathbf{i}, \mathbf{k} \in \{1, \dots, n\}^3, \quad (20)$$

and $H = T + V$, where T is the kinetic energy and V is the potential-energy operator in the perimetric coordinates. Our task is to find $E \in \mathbb{R}$ and $\mathcal{C} \in \mathbb{R}^{n \times n \times n}$ such that the tensor eigenvalue equation (19) holds true.

B. Generalized eigenvalue problem in specific tensor formats

We represent the generalized eigenvalue problem in the canonical format, the TT format, and the QTT format.

1. Generalized eigenvalue problem in canonical format

In our application, $M = N$ (see Definition 2), and therefore, $n_1 = n_2 = n_3 = n$ is the number of nodes per mode. To derive the canonical representation, exploiting the separation of variables, we expand the terms in Eqs. (20) into the sum of products of integrals. We give an example. Let $\mathbf{i} = (i_1, i_2, i_3)$ and $\mathbf{k} = (k_1, k_2, k_3) \in \{1, \dots, n\}^3$. Among the terms in Eq. (13), we need to compute

$$\left\langle xv_{jj} \frac{\partial L_{\mathbf{i}}}{\partial z_j}, \frac{\partial L_{\mathbf{k}}}{\partial z_j} \right\rangle, \quad j \in \{1, 2, 3\}.$$

As an example, for $j = 2$,

$$\begin{aligned} xv_{22} &= 4 \left(\frac{1}{m_1} + \frac{1}{m_3} \right) (z_1^2 z_2 + z_1 z_2^2) \\ &+ 4 \left(\frac{1}{m_1} + \frac{1}{m_2} \right) (z_2^2 z_3 + z_2 z_3^2) + \frac{8z_1 z_2 z_3}{m_1}, \end{aligned}$$

and we obtain

$$\begin{aligned}
\langle xv_{22}L_{i_1}L'_{i_2}L_{i_3}, L_{k_1}L'_{k_2}L_{k_3} \rangle &= 4\left(\frac{1}{m_1} + \frac{1}{m_3}\right) (\langle z_1^2L_{i_1}, L_{k_1} \rangle \langle z_2L'_{i_2}, L'_{k_2} \rangle \langle L_{i_3}, L_{k_3} \rangle \\
&\quad + \langle z_1L_{i_1}, L_{k_1} \rangle \langle z_2^2L'_{i_2}, L'_{k_2} \rangle \langle L_{i_3}, L_{k_3} \rangle) + 4\left(\frac{1}{m_1} + \frac{1}{m_2}\right) (\langle L_{i_1}, L_{k_1} \rangle \langle z_2^2L'_{i_2}, L'_{k_2} \rangle \langle z_3L_{i_3}, L_{k_3} \rangle) \\
&\quad + \langle L_{i_1}, L_{k_1} \rangle \langle z_2L'_{i_2}, L'_{k_2} \rangle \langle z_3^2L_{i_3}, L_{k_3} \rangle + \frac{8}{m_1} \langle z_1L_{i_1}, L_{k_1} \rangle \langle z_2L'_{i_2}, L'_{k_2} \rangle \langle z_3L_{i_3}, L_{k_3} \rangle.
\end{aligned} \tag{21}$$

See the Supplemental Material [38] for the full derivation. By introducing the matrices

$$\begin{aligned}
\mathbf{A}_1 &= [\langle L_i, L_j \rangle]_{i,j=1}^n, & \mathbf{A}_2 &= [\langle zL_i, L_j \rangle]_{i,j=1}^n, & \mathbf{A}_3 &= [\langle z^2L_i, L_j \rangle]_{i,j=1}^n, \\
\mathbf{B}_1 &= [\langle L'_i, L'_j \rangle]_{i,j=1}^n, & \mathbf{B}_2 &= [\langle zL'_i, L'_j \rangle]_{i,j=1}^n, & \mathbf{B}_3 &= [\langle z^2L'_i, L'_j \rangle]_{i,j=1}^n, \\
\mathbf{C}_1 &= [\langle L'_i, L_j \rangle]_{i,j=1}^n, & \mathbf{C}_2 &= [\langle zL'_i, L_j \rangle]_{i,j=1}^n, & \mathbf{C}_3 &= [\langle z^2L'_i, L_j \rangle]_{i,j=1}^n, \\
\mathbf{D}_1 &= [\langle L_i, L'_j \rangle]_{i,j=1}^n, & \mathbf{D}_2 &= [\langle zL_i, L'_j \rangle]_{i,j=1}^n, & \mathbf{D}_3 &= [\langle z^2L_i, L'_j \rangle]_{i,j=1}^n,
\end{aligned} \tag{22}$$

where z is equal to z_1 , z_2 , or z_3 and $\mathbf{A}_j, \mathbf{B}_j, \mathbf{C}_j, \mathbf{D}_j \in \mathbb{R}^{n \times n}$, $j \in \{1, 2, 3\}$, we can write the canonical representation of each tensor operator involved in the eigenvalue problem (19).

The canonical representation arising from the kinetic-energy operator can be expressed as

$$\begin{aligned}
\mathcal{T} &= 2\left(\frac{1}{m_3} + \frac{1}{m_2}\right) \mathbf{B}_3 \otimes \mathbf{A}_2 \otimes \mathbf{A}_1 + 2\left(\frac{1}{m_2} + \frac{1}{m_1}\right) \mathbf{B}_3 \otimes \mathbf{A}_1 \otimes \mathbf{A}_2 \\
&\quad + 2\left(\frac{1}{m_3} + \frac{1}{m_2}\right) \mathbf{B}_2 \otimes \mathbf{A}_3 \otimes \mathbf{A}_1 + 2\left(\frac{1}{m_2} + \frac{1}{m_1}\right) \mathbf{B}_2 \otimes \mathbf{A}_1 \otimes \mathbf{A}_3 \\
&\quad + 2\left(\frac{1}{m_3} + \frac{1}{m_1}\right) \mathbf{A}_3 \otimes \mathbf{B}_2 \otimes \mathbf{A}_1 + 2\left(\frac{1}{m_3} + \frac{1}{m_1}\right) \mathbf{A}_2 \otimes \mathbf{B}_3 \otimes \mathbf{A}_1 \\
&\quad + 2\left(\frac{1}{m_1} + \frac{1}{m_2}\right) \mathbf{A}_1 \otimes \mathbf{B}_3 \otimes \mathbf{A}_2 + 2\left(\frac{1}{m_1} + \frac{1}{m_2}\right) \mathbf{A}_1 \otimes \mathbf{B}_2 \otimes \mathbf{A}_3 \\
&\quad + 2\left(\frac{1}{m_3} + \frac{1}{m_1}\right) \mathbf{A}_3 \otimes \mathbf{A}_1 \otimes \mathbf{B}_2 + 2\left(\frac{1}{m_3} + \frac{1}{m_1}\right) \mathbf{A}_2 \otimes \mathbf{A}_1 \otimes \mathbf{B}_3 \\
&\quad + 2\left(\frac{1}{m_3} + \frac{1}{m_2}\right) \mathbf{A}_1 \otimes \mathbf{A}_3 \otimes \mathbf{B}_2 + 2\left(\frac{1}{m_3} + \frac{1}{m_2}\right) \mathbf{A}_1 \otimes \mathbf{A}_2 \otimes \mathbf{B}_3 \\
&\quad + \frac{4}{m_2} \mathbf{B}_2 \otimes \mathbf{A}_2 \otimes \mathbf{A}_2 + \frac{4}{m_1} \mathbf{A}_2 \otimes \mathbf{B}_2 \otimes \mathbf{A}_2 + \frac{4}{m_3} \mathbf{A}_2 \otimes \mathbf{A}_2 \otimes \mathbf{B}_2 \\
&\quad - \frac{2}{m_3} \mathbf{C}_3 \otimes \mathbf{D}_2 \otimes \mathbf{A}_1 - \frac{2}{m_3} \mathbf{C}_2 \otimes \mathbf{D}_3 \otimes \mathbf{A}_1 - \frac{2}{m_3} \mathbf{D}_3 \otimes \mathbf{C}_2 \otimes \mathbf{A}_1 \\
&\quad - \frac{2}{m_3} \mathbf{D}_2 \otimes \mathbf{C}_3 \otimes \mathbf{A}_1 - \frac{2}{m_2} \mathbf{A}_1 \otimes \mathbf{C}_3 \otimes \mathbf{D}_2 - \frac{2}{m_2} \mathbf{A}_1 \otimes \mathbf{C}_2 \otimes \mathbf{D}_3 \\
&\quad - \frac{2}{m_2} \mathbf{A}_1 \otimes \mathbf{D}_3 \otimes \mathbf{C}_2 - \frac{2}{m_2} \mathbf{A}_1 \otimes \mathbf{D}_2 \otimes \mathbf{C}_3 - \frac{2}{m_1} \mathbf{C}_3 \otimes \mathbf{A}_1 \otimes \mathbf{D}_2 \\
&\quad - \frac{2}{m_1} \mathbf{C}_2 \otimes \mathbf{A}_1 \otimes \mathbf{D}_3 - \frac{2}{m_1} \mathbf{D}_3 \otimes \mathbf{A}_1 \otimes \mathbf{C}_2 - \frac{2}{m_1} \mathbf{D}_2 \otimes \mathbf{A}_1 \otimes \mathbf{C}_3.
\end{aligned} \tag{23}$$

It has a canonical rank of 27. The representation arising from the potential-energy operator is given by

$$\begin{aligned}
\mathcal{V} &= 2(Z_1Z_2 + Z_2Z_3 + Z_3Z_1)(\mathbf{A}_1 \otimes \mathbf{A}_2 \otimes \mathbf{A}_2 + \mathbf{A}_2 \otimes \mathbf{A}_1 \otimes \mathbf{A}_2 + \mathbf{A}_2 \otimes \mathbf{A}_2 \otimes \mathbf{A}_1) \\
&\quad + 2Z_1Z_2\mathbf{A}_1 \otimes \mathbf{A}_1 \otimes \mathbf{A}_3 + 2Z_3Z_1\mathbf{A}_3 \otimes \mathbf{A}_1 \otimes \mathbf{A}_1 + 2Z_2Z_3\mathbf{A}_1 \otimes \mathbf{A}_3 \otimes \mathbf{A}_1.
\end{aligned} \tag{24}$$

It has a canonical rank of 6 (as the prefactor is a constant for a given system). Finally, the representation of the overlap operator is of canonical rank 7:

$$\begin{aligned}
\mathcal{S} &= \mathbf{A}_1 \otimes \mathbf{A}_2 \otimes \mathbf{A}_3 + \mathbf{A}_1 \otimes \mathbf{A}_3 \otimes \mathbf{A}_2 + \mathbf{A}_2 \otimes \mathbf{A}_1 \otimes \mathbf{A}_3 + \mathbf{A}_2 \otimes \mathbf{A}_3 \otimes \mathbf{A}_1 \\
&\quad + 2\mathbf{A}_2 \otimes \mathbf{A}_2 \otimes \mathbf{A}_2 + \mathbf{A}_3 \otimes \mathbf{A}_1 \otimes \mathbf{A}_2 + \mathbf{A}_3 \otimes \mathbf{A}_2 \otimes \mathbf{A}_1.
\end{aligned} \tag{25}$$

Here \otimes denotes the Kronecker product for matrices, so from the canonical format of an operator we can derive its full representation belonging to $\mathbb{R}^{n^3 \times n^3}$, where n is the number of nodes per mode.

2. Generalized eigenvalue problem in TT format

To transform our canonical representation to the TT representation, we refer to Sec. 3.1 in Oseledets [30]. In our application, $M = N$, and therefore, $\mathbb{R}^{N \times N} = \mathbb{R}^{(n \times n) \times (n \times n) \times (n \times n)}$ because each factor is an element of $\mathbb{R}^{n \times n}$. For example, from the canonical format of the overlap operator in Eq. (25) and by choosing the TT rank to be the canonical rank of the operator, we can write (6) as

$$\mathcal{S} = \mathcal{S}^{(1)} \otimes \mathcal{S}^{(2)} \otimes \mathcal{S}^{(3)}, \quad (26)$$

where

$$\mathcal{S}^{(1)} = [\mathbf{A}_1 \ \mathbf{A}_1 \ \mathbf{A}_2 \ \mathbf{A}_2 \ 2\mathbf{A}_2 \ \mathbf{A}_3 \ \mathbf{A}_3], \quad (27)$$

$$\mathcal{S}^{(2)} = \begin{bmatrix} \mathbf{A}_2 & \mathbf{0} & \mathbf{0} & \mathbf{0} & \mathbf{0} & \mathbf{0} & \mathbf{0} \\ \mathbf{0} & \mathbf{A}_3 & \mathbf{0} & \mathbf{0} & \mathbf{0} & \mathbf{0} & \mathbf{0} \\ \mathbf{0} & \mathbf{0} & \mathbf{A}_1 & \mathbf{0} & \mathbf{0} & \mathbf{0} & \mathbf{0} \\ \mathbf{0} & \mathbf{0} & \mathbf{0} & \mathbf{A}_3 & \mathbf{0} & \mathbf{0} & \mathbf{0} \\ \mathbf{0} & \mathbf{0} & \mathbf{0} & \mathbf{0} & \mathbf{A}_2 & \mathbf{0} & \mathbf{0} \\ \mathbf{0} & \mathbf{0} & \mathbf{0} & \mathbf{0} & \mathbf{0} & \mathbf{A}_1 & \mathbf{0} \\ \mathbf{0} & \mathbf{0} & \mathbf{0} & \mathbf{0} & \mathbf{0} & \mathbf{0} & \mathbf{A}_2 \end{bmatrix},$$

$$\mathcal{S}^{(3)} = \begin{bmatrix} \mathbf{A}_3 \\ \mathbf{A}_2 \\ \mathbf{A}_3 \\ \mathbf{A}_1 \\ \mathbf{A}_2 \\ \mathbf{A}_2 \\ \mathbf{A}_1 \end{bmatrix}. \quad (28)$$

The TT operator cores for \mathcal{T} and \mathcal{V} are provided in the Supplemental Material [38].

3. QTT format

If, as in our case, $n_1 = n_2 = n_3 = n$ (the number of nodes) for a third-order tensor operator, then we can express n as the product of several smaller numbers, viz.,

$$n = p_1 \times p_2 \times \cdots \times p_q, \quad (29)$$

which provides us with the opportunity to subdivide each core into multiple smaller cores (see Fig. 3). In this work we choose (29) to be a prime decomposition.

In Table I the complexities of the TT format and the QTT format for the operators \mathcal{T} , \mathcal{V} , and \mathcal{S} are compared to the complexity of the same tensor operators in the full format [21,31].

4. ALS algorithm

There are different ways to approach the eigenvalue problem in the TT format. We rely on the ALS algorithm, which can be regarded as a one-site DMRG-type algorithm. The

TABLE I. The complexity of the third-order tensor operators \mathcal{H} and \mathcal{S} , for which the maximum TT rank is 33, arising from \mathcal{H} , $p = \max_{1 \leq i \leq q} p_i$, where q and p_i are defined in (29).

Format	Storage complexity
Full	$\mathcal{O}(n^6)$
TT	$\mathcal{O}(3 \times 33^2 \times n^2)$
QTT	$\mathcal{O}(3 \times 33^2 \times \log_p n^2)$

ALS algorithm developed by Holtz *et al.* [19] to treat optimization problems in the TT format was inspired by the relaxation idea in alternating least squares, wherein all indices except one is fixed. In doing so, the multilinear parametrization in the TT form reduces to a linear parametrization in the free index. In conjunction with a stabilization technique (QR decomposition), a stable algorithm is obtained. ALS operates only on a TT manifold with fixed ranks, and as a consequence, it does not involve the truncation of TT decompositions. The complexity of the ALS algorithm for eigenvalue problems is $\mathcal{O}(b\gamma dr^3 R^2 n^2)$ [21], where d denotes the order of the involved tensors, n is the maximum of all mode lengths, r and R are the maximum TT ranks of tensor trains in \mathbb{R}^N and of TT operators in $\mathbb{R}^{N \times N}$, respectively, γ is the number of iterations of the iterative solvers for the microeigenvalue problems, and b is the number of eigenvalues and eigenvectors to be computed; in particular, in our work, the complexity is $\mathcal{O}(3\gamma 33^2 r^3 n^2)$, as 3 is the order of the tensors, 33 is the maximum TT rank of the tensor operators involved, b is set to 1, and n , r , and γ are chosen in the calculation.

C. Implementation

All calculations (canonical-derived full format, TT, and QTT) require as input the tensor format of the operators, which are expressed in terms of the factor matrices $\in \mathbb{R}^{n \times n}$ defined in (22). The numerical integration required for the factor matrices was performed using the `vpaintegral` command in MATLAB [24] because it allows for variable-precision arithmetic. For each calculation, the number of nodes n for each mode and the cutoff parameter z_c need to be defined. To obtain accurate energies it was necessary to decrease the default integration tolerances of `vpaintegral` (`AbsTol` = 10^{-10} and `Reltol` = 10^{-6}) for the numerical integration of the factor matrices to prevent large fluctuations in the energy calculations. Figure 4 shows the energy convergence obtained using three different integration schemes for helium, with the number of nodes n equal to the cutoff z_c corresponding to a density of $n/z_c = 1$ and using the QTT method with a fixed rank. Using helium with an infinite nucleus mass gave similar results, and the data are provided in the Supplemental Material [38]. It is shown that the large fluctuations using the default precision tolerances for `vpaintegral` were minimized by increasing the integration tolerance to 10^{-32} , indicating that the errors were numerical in nature. However, as the energies converged towards higher numerical accuracy, small fluctuations in the energy calculations were again observed. Although MATLAB is able to perform high-precision numerical integration, the software uses double-precision arithmetic, and it appeared that precision was lost when using other

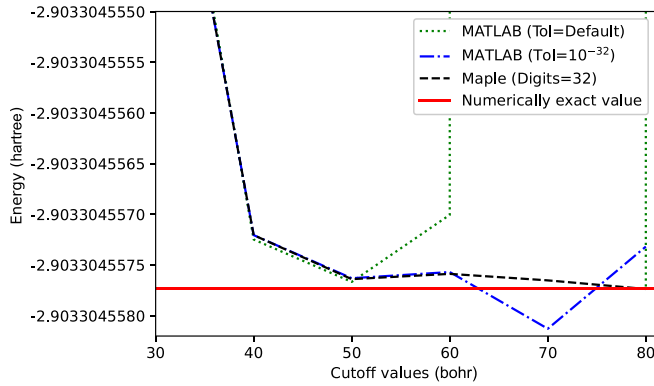


FIG. 4. The energy convergence for ^4He using different integration methods to calculate the factors required for the tensor format. Energies are calculated using QTT with rank 20, convergence threshold $\epsilon = 10^{-16}$, and node density $n/z_c = 1$.

functions. This was addressed somewhat (see Fig. 4) by calculating the integrals using the `int` command of MAPLE [39] with the `_Gquad` command and the precision set to 32 digits; `_Gquad` is an adaptive Gaussian quadrature method suitable for one-dimensional numerical integration which can be used in MAPLE’s arbitrary-precision software floating-point mode. MATLAB or MAPLE was chosen for ease of computation, but calculations using arbitrary precision could be implemented using, for example, PYTHON or C if greater precision is required in the future. The calculation of the factor matrices is the most time-consuming process and scales poorly with increasing n . Given that our code used to calculate the energy using TT or QTT is implemented in double precision and given that the MATLAB calculations were considerably faster than the MAPLE calculations, the results presented here use integrals calculated using `vpaintegral` with integration tolerances set to 10^{-32} . The Supplemental Material [38] shows that the energies presented in Sec. V converge monotonically to an upper bound of the energy and were not subject to fluctuations at that level of accuracy. The time taken to calculate the factor matrices ranges from 5696 s for $n = 42$ and $z_c = 24$ to 114 793 s for $n = 72$ and $z_c = 30$. However, the time taken to calculate the factor matrices is not included in the CPU time comparison presented in the next section as this step is required for all calculations and is thus independent of the tensor format chosen to solve the generalized eigenvalue problem (19).

Once the factors have been calculated, they are used to solve (19). From the canonical format of the operators, Eqs. (23), (24), and (25), the full representation can be derived by executing the tensor multiplication, where \otimes denotes the Kronecker product for matrices and each operator in the full representation belongs to $\mathbb{R}^{n^3 \times n^3}$. The resulting generalized eigenvalue problem is solved using the built-in `eig` command in MATLAB. The calculations are defined by the cutoff z_c and the number of nodes n per mode. Thus, the total number of nodes per calculation in the truncated domain Ω is n^3 , and the density of nodes for each mode is given by n/z_c . The limiting factor in the calculations using the full format is n ; in this work, using MATLAB, the maximum value of n is 42. The code was subsequently rewritten in PYTHON, and the generalized

TABLE II. Mass values (in a.u.) used in this work and previous work. Here “n/a” means not applicable.

Reference	Mass of ^1H	Mass of $^4\text{He}^{2+}$
This work, CODATA (2018) [40]	1836.152 673 43	7294.299 541 42
King <i>et al.</i> (2015) [41]	1836.152 672 45	7294.299 536 1
Frolov (2007) [42]	n/a	7294.299 536 3
Frolov (2002, 1998) [43,44]	1836.152 701	n/a
Ackermann and Shertzer (1996) [10]	1836.152 701	7294.299 62

eigenvalue problem was solved using the `eigs` command, but it was still not possible to extend n significantly, given that the full representation for an operator belongs to $\mathbb{R}^{n^3 \times n^3}$. Therefore, we use the PYTHON implementation with $n = 42$ as the benchmark when comparing the full format with the low-rank decompositions.

To perform TT and QTT calculations a PYTHON code was written which uses the tensor train toolbox `SCIKIT_TT` developed by Gelß *et al.* [20]. First, the tensor-train cores are derived from the canonical form for each operator. An example of the tensor-train cores for the identity operator is shown in Eqs. (27) and (28). `SCIKIT_TT` provides the ALS algorithm (see Sec. IV B 4). This algorithm is a variant of the one-site DMRG algorithm; therefore, for a specified rank it optimizes the tensor train. A series of calculations with varying tensor ranks r was performed to optimize the performance in terms of accuracy and computational cost. The convergence threshold ϵ was set to 10^{-16} , and the maximum number of iterations (sometimes referred to as sweeps) was set to 100.

The `SCIKIT_TT` toolbox also has the functionality to convert from the TT format to the QTT format. For this a prime decomposition of the number of nodes per mode was used to construct the “quantized” tensors in smaller cores (see Fig. 3). For each calculation, a suitable rank for the initial guess was chosen to ensure accurate results. Due to the effective low-rank decomposition of the tensor format using TT and QTT, which reduces the computational complexity, no restriction on the number of nodes was necessary.

All numerical computations were performed using PYTHON version 3.10.9 on a Precision 5820 Tower DELL computer with 256 GB RAM and an Intel Xeon Processor W-2295 (18 cores at 3 GHz).

V. RESULTS AND DISCUSSION

Calculations were performed on the helium atom (with finite and infinite nuclear masses), the positronium negative ion, and the H_2^+ molecule to demonstrate the applicability and versatility of this numerical-tensor-method approach to solving fully correlated all-particle Coulomb systems. The mass of the proton and that of the helium nucleus, relative to the electron mass, used in the present work are provided in Table II, along with the masses used in previous work. Energy convergence was established by comparing with literature values and data obtained using the method detailed in [15] with the latest committee on data for science and

TABLE III. The CPU time taken to calculate the ground-state energies for the all-particle systems He, Ps^- , and H_2^+ using the full, TT, and QTT tensor formats with the optimum node density n/z_c determined using the full representation. Energies are accurate to the number of digits reported.

	Format	Energy (hartree)	n	z_c (bohr)	Rank	CPU time (s)
He	Full	-2.903 304 557 7	42	24		9627
	TT	-2.903 304 557 7	42	24	8	6862
	QTT	-2.903 304 557 7	42	24	13	260
Ps^-	Full	-0.262 005 070	42	155		25 849
	TT	-0.262 005 070	42	155	7	2349
	QTT	-0.262 005 070	42	155	14	245
H_2^+	Full	-0.597 139 0	42	17		100 682
	TT	-0.597 139 0	42	17	11	34 020
	QTT	-0.597 139 0	42	17	20	2425

technology (CODATA) values [40], which are capable of picohartree accuracy and use quadruple precision.

Initially, we focus on the results obtained using the canonical-derived full format. For each calculation, the cutoff value z_c and the number of nodes n for each mode are defined. For each value of z_c , the impact of increasing the density of nodes per mode n/z_c on the accuracy of the computed energy and the rate of convergence was investigated. We found that increasing the density of nodes increases the accuracy of the energy, and for a fixed density, the accuracy increases with increasing z_c values. However, initial tests on atomic systems revealed that for small values of z_c with a large density of nodes the energies obtained were nonvariational; i.e., they were lower than the exact value. A similar dependence on the cutoff parameter was found by Ackermann [9,10], who reported that eigenvalues were artificially lowered when the cutoff values were small. The z_c value required to prevent the appearance of spurious energies is system dependent; see the Supplemental Material [38] for further details. Therefore, it was important to ensure that z_c was sufficiently large for the given system.

The number of nodes n per mode that was feasible using the full canonical-derived format was 42. Therefore, the best results for each system with $n = 42$ are provided in Table III. There are subtle differences in the three types of systems. For the helium atom (with or without an infinite nuclear mass), the node density was the most influential factor affecting accuracy. The calculations converged quickly, and an energy accurate to greater than a nanohartree was obtained with $n = 42$ and a cutoff value of 24 bohrs, which corresponds to a node density of 1.75. For the positronium negative ion (like the hydride ion, not shown) a much greater cutoff value was required to achieve accuracy comparable to that of the helium atom. This is not unsurprising as Ps^- has a loosely bound electron and the system is more diffuse and thus has a greater radial extent; therefore, a larger domain is required to capture the physics of this system. As the value of n is capped at 42, this results in a very low node density of 0.27, yet an impressive nanohartree accuracy is still obtainable. For the non-BO molecular system, H_2^+ , convergence is slower, and significantly greater CPU time is required (see

TABLE IV. QTT energies for He, Ps^- , and H_2^+ , accurate to the number of digits reported.

	Format	Energy (hartree)	n	z_c (bohr)	Rank	CPU time (s)
He	QTT	-2.903 304 557 72	54	45	15	555
Ps^-	QTT	-0.262 005 070 23	54	190	15	895
H_2^+	QTT	-0.597 139 063 0	72	30	18	1484

Table III). This slower convergence for molecular systems compared to atomic systems was reported before [45], and the increase in numerical work required to reach a certain precision as the masses of the two heavy particles increases was also noted [10]; these features are attributed to the use of interparticle distances. The Hamiltonian contains operators of the nuclear coordinates as well as the electron coordinates; however, a benefit is that the solution automatically includes nuclear motions such as molecular vibrations together with the electron motions. For reasonable accuracy a high node density is required. With n fixed at 42 it was possible to obtain submicrohartree accuracy.

Next, we focus on demonstrating the utility of low-rank tensor decompositions for solving a fully correlated Coulomb system. Table III shows the best energies obtained using the tensor-train format with the same number of nodes and cutoff as in the full representation to give a direct comparison. The TT rank was varied until the same accuracy as that obtained in the full representation was achieved. It is shown that for all three types of systems (atomic, exotic, and molecular) the TT significantly reduces the CPU times required to solve the generalized eigenvalue problem (19) without compromising the accuracy. This is achieved with a TT rank of 8 for the He calculation, a rank of 7 for the Ps^- calculation, and a slightly higher rank of 11 for the H_2^+ calculation. However, given that the maximum of the TT rank of the initial guess is bounded by n , as a consequence of the TT singular-value decomposition [30] and Theorem 1 of [46], this is a surprisingly small rank and demonstrates the effectiveness of the ALS algorithm in constructing the microsystems (cores) and solving the low-dimensional eigenvalue problems. The same approach was taken to determine the effectiveness of the QTT approach; i.e., n and z_c were fixed at the optimum values for the full representation. The QTT rank was varied to determine whether it was possible to obtain the same accuracy as in the full representation. It was found that, with a slightly higher rank than that needed for the TT calculation, energies with the same accuracy as in the full representation were gained. Furthermore, the CPU time was reduced by an order of magnitude in all cases. This result is perhaps quite surprising because information is necessarily lost when performing such low-rank decompositions, but these results demonstrate that, with a suitably chosen rank and using the efficient ALS algorithm, it is possible to obtain high-accuracy results.

For TT and QTT there is no restriction on the number of nodes permissible due to the reduction in computational complexity, and Table IV shows that the accuracy can be pushed further, if desired, by increasing the number of nodes and/or the cutoff parameter. The prime decomposition of n

TABLE V. Expectation values $\langle X_i \rangle$ (in a.u.), of some bound-state properties for the ground states of He, Ps^- , and H_2^+ using the QTT format, accurate to the number of digits reported. A subscript 1 designates the nucleus-electron interaction, and 12 denotes the interaction between the like-charged particles.

Property	He	Ps^-	H_2^+
$\langle r_1 \rangle$	0.929 607 915 01	5.489 633 25	1.692 966 208
$\langle r_{12} \rangle$	1.422 247 512 6	8.548 580 65	2.063 913 86
$\langle r_1^{-1} \rangle$	1.688 076 584 6	0.339 821 023	0.842 492 96
$\langle r_{12}^{-1} \rangle$	0.945 697 223 2	0.155 631 9	0.490 707 79
$\langle r_1^2 \rangle$	1.193 834 894	48.418 937	3.558 797 930
$\langle r_{12}^2 \rangle$	2.517 061 842	93.178 633 8	4.313 285 94
$\langle \delta(r_1) \rangle$	1.809 672	0.020 733 1	0.206 736
$\langle \delta(r_{12}) \rangle$	0.106 (300) ^a	0.000 170 99	$3.37 \times 10^{-9\text{b}}$
η	2.89×10^{-10}	8.7×10^{-10}	3.2×10^{-9}
ν_1^{c}	-1.999 725	-0.500 000	-0.9994
ν_{12}^{d}	0.500 00	0.500 00	-106.759 ^b

^aThe digits in parentheses do not agree with the literature, which we attribute to the difference in masses used.

^bThis value does not agree with literature values; see text for details.

^cThe exact value of ν_1 for ^4He to nine decimal places is $-1.999\,725\,851$, for Ps^- it is -0.5 , and for H_2^+ it is $-0.999\,455\,679$.

^dThe exact value of ν_{12} for ^4He and Ps^- is 0.5 , and for H_2^+ it is $918.076\,336$.

used to construct the QTT cores plays a key role in reducing the CPU time. For example choosing $n = 55 = 5 \times 11$ takes 3 times longer than $n = 54 = 2 \times 3^3$ when $z_c = 45$ (for He) and 13 times longer when $z_c = 190$ (for Ps^-). Similarly, choosing $n = 75 = 3 \times 5^2$ takes nearly 2.5 times longer than $n = 72 = 2^3 \times 3^2$ when $z_c = 30$ (for H_2^+).

Furthermore, our numerical tensor method determines not only the ground-state energy but also excited-state energies. The higher roots after diagonalization correspond to the excited states. For example, for the H_2^+ system reported in Table IV, the second and third eigenvalues are equal to $-0.587\,155\,679\,0$ Ha and $-0.577\,751\,904$ Ha, respectively, in good agreement with other high-level calculations (see, for example, [47]). An advantage of these non-BO calculations is that the difference between eigenvalues captures the effects of nuclear motion. For example, the difference between the first and second eigenvalues and the difference between the second and third eigenvalues correspond to the frequency for H_2^+ between $v = 0$ and 1 and $v = 1$ and 2, respectively. The calculated frequencies are 2191.0995 and 2063.8900 cm^{-1} , which are in excellent agreement with the experimental values of 2191.2 ± 0.2 and 2064.2 ± 0.2 cm^{-1} , respectively [48]. The slightly smaller value for the latter reflects the anharmonicity of the vibrational motions.

A key consideration regarding the applicability of a new method is the quality of the wave function obtained. This is because many applications involve the calculation of expectation values and/or matrix elements, for example, relativistic and quantum electrodynamics (QED) corrections. Table V provides expectation values calculated using the QTT wave functions corresponding to the energies and parameters (n , z_c , and rank) reported in Table IV. The data reported in Ta-

ble V are accurate to the number of digits presented. The ^4He results are compared with results from [41,42]. The older masses used in [41,42] agree with the latest mass values [40] to eight significant figures (see Table II). The H_2^+ results are compared with those from [43,44]; the ^1H masses used in [43,44] agree to seven significant figures compared with the values used in this work. To further check, calculations were also performed using the series-solution method described in [15] with the latest CODATA mass values [40]. The Ps^- results were compared with the results of Frolov [49]. All of the expectation values of the interparticle distances are accurate to at least seven significant figures, and those for He are accurate to ≥ 10 significant figures. However, the two-particle delta functions $\delta(r_i)$ (where a subscript 1 refers to the nucleus-electron interaction and a subscript 12 refers to the interaction between like-charged particles, i.e., the electron-electron interaction in He and Ps^- and the nucleus-nucleus interaction in H_2^+) are less accurate. In general, the δ functions are accurate to approximately six significant figures, but the nucleus-nucleus δ function is at least an order of magnitude less than the values reported by Frolov of 4.44×10^{-10} [44] and 1.405×10^{-13} [43]. Also provided in Table V are two-body cusp ratios, determined using [44,50]

$$\nu_{ij} = \langle \hat{\nu}_{ij} \rangle = \frac{\langle \delta(r_{ij}) \frac{\partial}{\partial r_{ij}} \rangle}{\langle \delta(r_{ij}) \rangle} \quad (30)$$

and compared to the exact value given by $Z_i Z_j \frac{m_i m_j}{m_i + m_j}$. The nucleus-electron cusps ν_1 and the electron-electron cusps ν_{12} for He and Ps^- are accurate to at least five significant figures. However, the nuclear-nuclear cusp ν_{12} for H_2^+ is significantly less accurate than other bound-state properties and does not agree with the exact value. This was noted in previous work on adiabatic three-body systems [43,51,52], where the computed nuclear-nuclear cusps and nuclear-nuclear δ functions differed significantly from the predicted values. An explanation was provided in [43,51], namely, that the expansion of the wave function in interparticle coordinates cannot successfully reproduce the nuclear-nuclear cusp property corresponding to the very short internuclear distances. Finally, the extent to which the virial condition $\langle \hat{V} \rangle = -2\langle \hat{T} \rangle$ is satisfied provides a measure of the quality of the solution. It was found that for all systems, the virial factor η , defined as

$$\eta = \left| \frac{\langle \hat{V} \rangle}{\langle \hat{T} \rangle} + 2 \right|, \quad (31)$$

where $\langle \hat{V} \rangle$ and $\langle \hat{T} \rangle$ are the expectation values of the potential and kinetic energies, respectively, was less than $\sim 10^{-9}$, which is close to the exact value of zero.

VI. CONCLUSION

In this paper we have used a finite-element approach in combination with a low-rank tensor-decomposition ansatz to derive canonical, TT, and QTT tensor formats for all-particle three-body Coulomb systems. We showed that the derived tensor formats reduce the CPU time taken to perform the calculation without compromising the accuracy of the

energies obtained and that the QTT tensor method is the most computationally efficient and can provide reasonable expectation values, demonstrating the quality of the wave function. For all three types of systems considered (atomic, exotic, and molecular) energies converged to an accuracy greater than a nanohartree in less than 30 min on a standard PC. However, a computational bottleneck is the calculation of the factor matrices (which are not included in the CPU time presented for solving the generalized eigenvalue problem in tensor format because they are required for all formulations), and they require high precision in order to achieve results accurate to the nanohartree or better. This work demonstrates the utility of numerical tensor methods for all-particle treatments that go beyond the standard orbital and BO approximations used in conventional QC. Future work will focus on alternative formulations that address the factor-matrix

bottleneck and further improve the reduction in computational complexity.

ACKNOWLEDGMENTS

H.C. and M.M. would like to thank the Royal Society for the award of an APEX grant (Grant No. APX/R1/211226) funded by the Leverhulme Trust, British Academy, Royal Academy of Engineering and Royal Society. H.C. and K.T.B. would like to thank the Engineering and Physical Sciences Research Council (EPSRC) for the award of a Ph.D. studentship to K.T.B. (Training Grant No. EP/R513362/1). The authors would also like to thank MChem student P. Russell, who contributed towards preliminary results on model systems; Dr. Y. Petrov for helpful discussions on the FEM method; and Dr. P. Gelß regarding the SCIKIT_TT toolbox [20].

-
- [1] R. Olivares-Amaya, W. Hu, N. Nakatani, S. Sharma, J. Yang, and G. K. Chan, The *ab-initio* density matrix renormalization group in practice, *J. Chem. Phys.* **142**, 034102 (2015).
- [2] U. Schollwöck, The density-matrix renormalization group in the age of matrix product states, *Ann. Phys. (NY)* **326**, 96 (2011).
- [3] U. Schollwöck, The density-matrix renormalization group: A short introduction, *Philos. Trans. R. Soc. A* **369**, 2643 (2011).
- [4] A. Baiardi and M. Reiher, The density matrix renormalization group in chemistry and molecular physics: Recent developments and new challenges, *J. Chem. Phys.* **152**, 040903 (2020).
- [5] G. Catarina and B. Murta, Density-matrix renormalization group: A pedagogical introduction, *Eur. Phys. J. B* **96**, 111 (2023).
- [6] W. K. Ford and F. S. Levin, Channel-coupling theory of molecular structure. Finite-element method solution for H_2^+ , *Phys. Rev. A* **29**, 43 (1984).
- [7] F. S. Levin and J. Shertzer, Finite-element solution of the Schrödinger equation for the helium ground state, *Phys. Rev. A* **32**, 3285 (1985).
- [8] J. Shertzer and F. S. Levin, Solution of three-body Coulomb problems for $J = 0$, *Phys. Rev. A* **43**, 2531 (1991).
- [9] J. Ackermann, Finite-element-method expectation values for correlated two-electron wave functions, *Phys. Rev. A* **52**, 1968 (1995).
- [10] J. Ackermann and J. Shertzer, Finite-element calculations for the three-body Coulomb problem with two equal masses, *Phys. Rev. A* **54**, 365 (1996).
- [11] L. E. Ratcliff, W. Dawson, G. Fiscaro, D. Caliste, S. Mohr, A. Degomme, B. Videau, V. Cristiglio, M. Stella, M. D'Alessandro, S. Goedecker, T. Nakajima, T. Deutsch, and L. Genovese, Flexibilities of wavelets as a computational basis set for large-scale electronic structure calculations, *J. Chem. Phys.* **152**, 194110 (2020).
- [12] P. Motamarri, S. Das, S. Rudraraju, K. Ghosh, D. Davydov, and V. Gavini, DFT-FE - A massively parallel adaptive finite-element code for large-scale density functional theory calculations, *Comput. Phys. Commun.* **246**, 106853 (2020).
- [13] V. Khoromskaia and B. N. Khoromskij, *Tensor Numerical Methods in Quantum Chemistry* (De Gruyter, Berlin, Boston, 2018).
- [14] A. Veit and L. R. Scott, Using the tensor-train approach to solve the ground-state eigenproblem for hydrogen molecules, *SIAM J. Sci. Comput.* **39**, B190 (2017).
- [15] H. Cox and A. L. Baskerville, The series solution method in quantum chemistry for three-particle systems, *Adv. Quantum Chem.* **77**, 201 (2018).
- [16] E. Mátyus, Pre-Born–Oppenheimer molecular structure theory, *Mol. Phys.* **117**, 590 (2019).
- [17] J. Mitroy, S. Bubin, W. Horiuchi, Y. Suzuki, L. Adamowicz, W. Cencek, K. Szalewicz, J. Komasa, D. Blume, and K. Varga, Theory and application of explicitly correlated Gaussians, *Rev. Mod. Phys.* **85**, 693 (2013).
- [18] H. Nakashima and H. Nakatsuji, Solving the electron-nuclear Schrödinger equation of helium atom and its isoelectronic ions with the free iterative-complement-interaction method, *J. Chem. Phys.* **128**, 154107 (2008).
- [19] S. Holtz, T. Rohwedder, and R. Schneider, The altering linear scheme for tensor optimization in the tensor train format, *SIAM J. Sci. Comput.* **34**, A683 (2012).
- [20] P. Gelß, S. Klus, M. Scherer, F. Nüske, and M. Lücke, SCIKIT-TT, https://github.com/PGelss/scikit_tt.
- [21] P. Gelß, The tensor-train format and its applications: Modeling and analysis of chemical reaction networks, catalytic processes, fluid flows, and Brownian dynamics, Ph.D. thesis, Freien Universität Berlin, 2017.
- [22] T. G. Kolda and B. W. Bader, Tensor decompositions and applications, *SIAM Rev.* **51**, 455 (2009).
- [23] W. Hackbusch, *Tensor Spaces and Numerical Tensor Calculus*, 2nd ed., Springer Series in Computational Mathematics, Vol. 56 (Springer, Cham, 2019).
- [24] MathWorks, MATLAB, version R2023a, Natick, MA, 2022.
- [25] V. de Silva and L.-H. Lim, Tensor rank and the ill-posedness of the best low-rank approximation problem, *SIAM J. Matrix Anal. Appl.* **30**, 1084 (2008).
- [26] G. Vidal, Efficient classical simulation of slightly entangled quantum computations, *Phys. Rev. Lett.* **91**, 147902 (2003).
- [27] U. Schollwöck, The density-matrix renormalization group, *Rev. Mod. Phys.* **77**, 259 (2005).

- [28] W. Hackbusch and S. Kühn, A new scheme for the tensor representation, *J. Fourier Anal. Appl.* **15**, 706 (2009).
- [29] I. V. Oseledets and E. E. Tyrtshnikov, Breaking the curse of dimensionality, or how to use SVD in many dimensions, *SIAM J. Sci. Comput.* **31**, 3744 (2009).
- [30] I. V. Oseledets, Tensor-train decomposition, *SIAM J. Sci. Comput.* **33**, 2295 (2011).
- [31] B. N. Khoromskij, $O(d \log N)$ -quantics approximation of $N - d$ tensors in high-dimensional numerical modeling, *Constr. Approximation* **34**, 257 (2011).
- [32] T. Kato, On the existence of solutions of the helium wave equation, *Trans. Am. Math. Soc.* **70**, 212 (1951).
- [33] E. C. Kemble, *The Fundamental Principles of Quantum Mechanics with Elementary Applications* (Dover, New York, 1958).
- [34] A. S. Coolidge and H. M. James, On the convergence of the Hylleraas variational method, *Phys. Rev.* **51**, 855 (1937).
- [35] B. T. Sutcliffe, The use of perimetric coordinates in the vibration-rotation Hamiltonian for triatomic molecules, *Mol. Phys.* **75**, 1233 (1992).
- [36] H. Cox, S. J. Smith, and B. T. Sutcliffe, Some calculations on the ground and lowest-triplet state of helium in the fixed-nucleus approximation, *Phys. Rev. A* **49**, 4520 (1994).
- [37] J. H. Mathews *et al.*, *Numerical Methods Using MATLAB* (Pearson Prentice Hall, Upper Saddle River, NJ, 2004), Vol. 4.
- [38] See Supplemental Material at <http://link.aps.org/supplemental/10.1103/PhysRevA.109.062812> for the full derivation, expectation value calculation details, the effect of cutoff and integral precision on energy convergence, and CPU time dependence on the prime decomposition of n for QTT.
- [39] Maplesoft, MAPLE, Waterloo, Ontario, Canada, 2022.
- [40] E. Tiesinga, P. J. Mohr, D. B. Newell, and B. N. Taylor, CODATA recommended values of the fundamental physical constants: 2018, *J. Phys. Chem. Ref. Data* **50**, 033105 (2021); physics.nist.gov/constants.
- [41] A. W. King, L. C. Rhodes, C. A. Readman, and H. Cox, Effect of nuclear motion on the critical nuclear charge for two-electron atoms, *Phys. Rev. A* **91**, 042512 (2015).
- [42] A. M. Frolov, Field shifts and lowest order QED corrections for the ground 1^1S and 2^3S states of the helium atoms., *J. Chem. Phys.* **126**, 104302 (2007).
- [43] A. M. Frolov, Structures and properties of the ground states in H_2^+ -like adiabatic ions, *J. Phys. B* **35**, L331 (2002).
- [44] A. M. Frolov, Two-stage strategy for high-precision variational calculations, *Phys. Rev. A* **57**, 2436 (1998).
- [45] A. W. King, F. Longford, and H. Cox, The stability of S-states of unit-charge Coulomb three-body systems: From H^- to H_2^+ , *J. Chem. Phys.* **139**, 224306 (2013).
- [46] S. Holtz, T. Rohwedder, and R. Schneider, On manifolds of tensors of fixed TT-rank, *Numer. Math.* **120**, 701 (2012).
- [47] Y. Hijikata, H. Nakashima, and H. Nakatsuji, Solving non-Born–Oppenheimer Schrödinger equation for hydrogen molecular ion and its isotopomers using the free complement method, *J. Chem. Phys.* **130**, 024102 (2009).
- [48] G. Herzberg and C. Jungen, Rydberg series and ionization potential of the H_2 molecule, *J. Mol. Spectrosc.* **41**, 425 (1972).
- [49] A. M. Frolov, Mass-dependencies of the bound state properties for three-body positronium-like excitonic complexes, *Eur. Phys. J. B* **93**, 87 (2020).
- [50] T. Kato, On the eigenfunctions of many-particle systems in quantum mechanics, *Commun. Pure Appl. Math.* **10**, 151 (1957).
- [51] A. M. Frolov, Bound state properties of the ground states in the DT^+ and T_2^+ ions, *Phys. Rev. E* **65**, 046705 (2002).
- [52] M. Hesse and D. Baye, Lagrange-mesh calculations of three-body atoms and molecules, *J. Phys. B* **32**, 5605 (1999).